

Black hole spectroscopy by mode cleaning

Sizheng Ma,^{1,*} Ling Sun,² and Yanbei Chen¹

¹*TAPIR 350-17, California Institute of Technology, 1200 E California Boulevard, Pasadena, CA 91125, USA*

²*OzGrav-ANU, Centre for Gravitational Astrophysics, College of Science, The Australian National University, ACT 2601, Australia*

(Dated: January 18, 2023)

We formulate a Bayesian framework to analyze ringdown gravitational waves from colliding binary black holes and test the no-hair theorem. The idea hinges on mode cleaning—revealing subdominant oscillation modes by removing dominant ones using newly proposed *rational filters*. By incorporating the filter into Bayesian inference, we construct a likelihood function that depends only on the mass and spin of the remnant black hole (no dependence on mode amplitudes and phases) and implement an efficient pipeline to constrain the remnant mass and spin without Markov chain Monte Carlo (MCMC). We test ringdown models by cleaning combinations of different modes and evaluating the consistency between the residual data and pure noise. The model evidence and Bayes factor are used to demonstrate the presence of a particular mode and to infer the mode starting time. In addition, we design a hybrid approach to estimate the remnant black hole properties exclusively from a single mode using MCMC after mode cleaning. We apply the framework to GW150914 and demonstrate more definitive evidence of the first overtone by cleaning the fundamental mode. This new framework provides a powerful tool for black hole spectroscopy in future gravitational-wave events.

Introduction.— The final stage of a binary black hole (BBH) coalescence corresponds to the formation of the remnant BH and its ringing down to a stationary state. The BH linear perturbation theory predicts that the gravitational wave (GW) emitted during this ringdown stage is a superposition of exponentially damped sinusoids called quasi-normal modes (QNMs) at complex frequencies ω_{lmn} [1–4], labeled by two angular numbers (l, m) and an overtone index n . These complex frequencies ω_{lmn} are fully determined by the mass and spin of the remnant BH due to the no-hair theorem [5–8], thereby leading to the program of *BH spectroscopy* [9–12]: the mass and spin of the remnant BH can be measured from the frequency and decay rate of any single QNM in the ringdown regime [9]; detecting multiple modes allows tests for the no-hair theorem [10–12].

A few decades after the conception of BH spectroscopy [9–38], the first GW detections of BBH mergers [39] made by Advanced LIGO [40–43] allowed the measurement of QNMs from real GW events, such as GW150914 [29, 31–36] and GW190521 [37, 38, 44]. At late enough times, the fundamental QNM was detected in GW150914 [31, 45], with the inferred mass and spin of the remnant BH consistent with the ones obtained from the full inspiral-merger-ringdown (IMR) signal. Giesler *et al.* [46] showed that in a waveform produced by numerical relativity, the ringdown regime starts as early as the time when the strain reaches its peak, if enough overtones are included. Motivated by Giesler *et al.* [46], Isi *et al.* [32] extended the ringdown analysis to earlier times, showing the evidence for the first overtone in GW150914 with a significance 3.6σ . Studies by Bustillo *et al.* [29] and Finch *et al.* [36] with different methods also support the existence of the first overtone but with weaker evidence. The conclusion was challenged by Cotesta *et al.* [34] and

then further clarified and discussed by Isi *et al.* [35]. Recently, the existence of the $(l = m = 3, n = 0)$ mode in the ringdown of GW190521 [37, 38, 44] is under debate.

A major complication in BH spectroscopy is the non-orthogonality of QNMs, which at low SNRs lead to much ambiguity regarding the existence of modes. Proposals [33, 36] have been put forward to solve this issue, including using posteriors of the remnant mass and spin, posteriors of the overtone amplitude, the Bayes factor as a function of analysis start time, and deviations from the overtone frequencies predicted by general relativity. We propose to address this by *mode cleaning*, which highlights the weaker QNMs of interest by removing stronger modes. This approach has proven fruitful for theoretical waveforms obtained from numerical relativity [47]. In this paper, a Bayesian framework allows us to apply these filters to real data, leading to more definite evidence for weaker QNMs. We will use GW150914 as an example for its application.

The rational filter.— In Ref. [47], we showed that QNM(s) can be removed using the so-called “rational filters”. Moreover, the presence of weaker modes in numerical-relativity ringdown waveforms, e.g., the second-order QNMs (also see [48, 49]) and retrograde modes, becomes more pronounced after removing the most dominant mode(s). Let us now clean a ω_{lmn} –QNM from time-series data d_t that contains both signal and noise. We first transform d_t to the frequency domain via fast Fourier transform (FFT), producing frequency-domain data \tilde{d}_f . Note that we typically set the length of d_t to be longer than the full IMR signal to avoid spectral leakage. We then apply a rational filter [47, 50]

$$\mathcal{F}_{lmn}(f; M_f, \chi_f) = \frac{2\pi f - \omega_{lmn}}{2\pi f - \omega_{lmn}^*} \frac{2\pi f + \omega_{lmn}^*}{2\pi f + \omega_{lmn}}, \quad (1)$$

to \tilde{d}_f . Finally, we transform the filtered frequency-domain

data back to the time domain, given by

$$d_t^F = \int df \tilde{d}_f \mathcal{F}_{lmn}(f) e^{-i2\pi ft}. \quad (2)$$

Multiple QNMs can be cleaned simultaneously via a product filter:

$$\mathcal{F}_{\text{tot}} = \prod_{lmn} \mathcal{F}_{lmn}. \quad (3)$$

The filtered time-series data d_t^F are still real-valued because each filter satisfies $\mathcal{F}_{lmn}(-f) = [\mathcal{F}_{lmn}(f)]^*$.

Since the filter \mathcal{F}_{lmn} operates on the entire data segment, we list its impact on different parts of the signal and noise. For the early inspiral part, the filter introduces a trivial phase and negative time shift [47], which has no influence on the ringdown analysis. When using \mathcal{F}_{lmn} to clean the ω_{lmn} mode, the amplitude of a different mode, $\omega_{l'm'n'}$ ($l \neq l'$ or $m \neq m'$ or $n \neq n'$), is reduced by a factor of $B_{lmn}^{l'm'n'}$, given by [50]

$$B_{lmn}^{l'm'n'} e^{i\varphi_{lmn}^{l'm'n'}} \equiv \mathcal{F}_{lmn}(\omega_{l'm'n'}). \quad (4)$$

The symmetry of \mathcal{F}_{lmn} in Eq. (1) yields an identity $B_{lmn}^{l'm'n'} = B_{l'm'n'}^{lmn}$. The start time and oscillation of the $\omega_{l'm'n'}$ mode remain unchanged. Finally, we emphasize that the filter has no impact on the statistical properties of the noise, including Gaussianity, stationarity, and the one-sided noise power spectral density (PSD), $S(f)$, because $|\mathcal{F}_{lmn}(f)| = 1$ for at any real frequencies [50].

Integrating the filter into Bayesian inference.— After cleaning enough QNMs using a total filter \mathcal{F}_{tot} [Eq. (3)], we expect the ringdown portion of the filtered data d_t^F to be consistent with pure noise. Thus we introduce a novel likelihood function in time domain [50], following the procedure in Ref. [33]

$$\ln P(d_t|M_f, \chi_f, t_0, \mathcal{F}_{\text{tot}}) = -\frac{1}{2} \sum_{ij} d_i^F C_{ij}^{-1} d_j^F, \quad (5)$$

where C_{ij} is the autocovariance function, and $d_i^F \equiv d^F(t_i)$ denotes the samples of the filtered data after some truncation time t_0 ($t_i > t_0$). For any given t_0 , the likelihood function depends only on two parameters: M_f and χ_f , which are used to construct the filter $\mathcal{F}_{\text{tot}}(M_f, \chi_f)$. There is no additional dependence on the amplitudes and phases of QNMs — the corresponding QNMs can be removed from the ringdown regime regardless of their amplitudes and phases. This is similar to the case where a constant can be removed by taking the derivative no matter what the value of the constant is. In other words, the new likelihood in Eq. (5) automatically marginalizes over the mode amplitude and phase, compared to the usual full-ringdown (full-RD) MCMC analysis that does not apply the rational filter (see Refs. [32, 33]). In the Appendix of our companion paper [50], we demonstrate the equivalence of Eq. (5) and the conventional likelihood function

by conducting such a marginalization explicitly under a large-SNR limit and show that our new approach has the same Cramér–Rao bound as the full-RD MCMC analysis [32, 33].

Since Eq. (5) is merely a two-dimensional (2D) function, the direct evaluation of the likelihoods is efficient enough such that we do not need random sampling techniques, e.g., Markov chain Monte Carlo. In addition, the likelihoods can be easily converted to the joint posteriors of M_f and χ_f via

$$\ln P(M_f, \chi_f|d_t, t_0, \mathcal{F}_{\text{tot}}) \propto \ln P(d_t|M_f, \chi_f, t_0, \mathcal{F}_{\text{tot}}) + \ln \Pi(M_f, \chi_f), \quad (6)$$

where $\ln \Pi(M_f, \chi_f)$ is the prior. We can obtain the one-dimensional (1D) distribution of χ_f and M_f via marginalization:

$$P(M_f|d_t, t_0, \mathcal{F}_{\text{tot}}) = \int P(M_f, \chi_f|d_t, t_0, \mathcal{F}_{\text{tot}}) d\chi_f, \quad (7)$$

$$P(\chi_f|d_t, t_0, \mathcal{F}_{\text{tot}}) = \int P(M_f, \chi_f|d_t, t_0, \mathcal{F}_{\text{tot}}) dM_f. \quad (8)$$

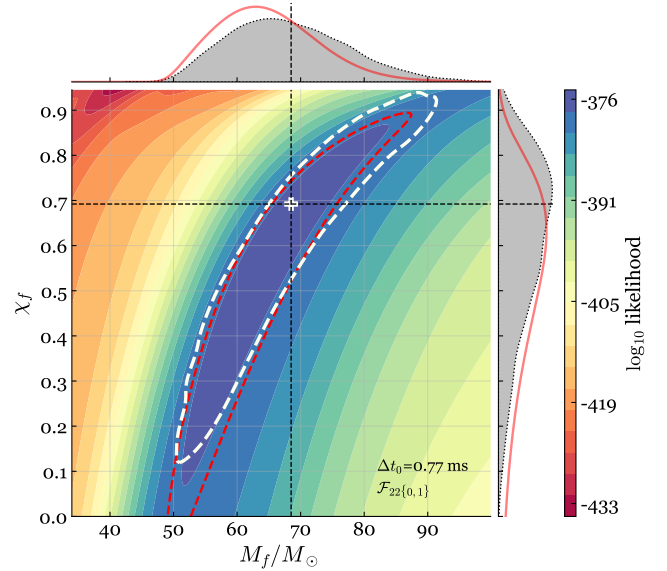


FIG. 1. Joint posterior distribution of M_f and χ_f [Eq. (6)] for GW150914. The red dashed contour displays the 90% credible region by integrating the joint posteriors. The analysis window starts at $\Delta t_0 = 0.77$ ms. The applied filter consists of both the fundamental mode and the first overtone. The white plus sign marks the full IMR estimates ($M_f^{\text{IMR}} = 68.5 M_\odot$, $\chi_f^{\text{IMR}} = 0.69$). The white dashed contour encloses 90% credible region obtained from the full-RD MCMC analysis presented in Refs. [32, 33]. In the side panels, 1D marginal distributions obtained from our new approach and the conventional full-RD MCMC analysis are shown in red and gray, respectively.

We demonstrate the analysis using the LIGO Hanford and Livingston data of GW150914 [39, 51, 52]. We set

the inferred GPS time at geocenter when the signal strain reaches the peak, $t_{\text{peak}} = 1126259462.4083$ [32], and parameterize the analysis starting time via $\Delta t_0 = t_0 - t_{\text{peak}}$. We use the PYTHON package `ringdown` [33, 53] to condition the data: (a) remove contents that are below 20 Hz via a high-pass filter, (b) remove direct current noise, and (c) downsample the data to 2048 Hz. We use the Welch method [54] to estimate the PSDs of the two detectors with a 32-s segment of the conditioned data. The PSDs are then converted to the autocovariance function C_{ij} . We align the signals at the two detectors using the sky position of this event [32]: right ascension $\alpha = 1.95$ rad and declination $\delta = -1.27$ rad. The information about the polarization and inclination angles is not needed in our framework. We fix the width of the ringdown analysis window to 0.2 s.

The joint posteriors of M_f and χ_f evaluated with Eq. (6) are shown as colored contours in Fig. 1. We set $\Delta t_0 = 0.77$ ms and choose a flat prior distribution. Both the fundamental mode and the first overtone are cleaned using the total filter $\mathcal{F}_{\text{tot}} = \mathcal{F}_{221}\mathcal{F}_{220}$. With the posteriors computed over the whole parameter space, we calculate the 90% credible region (red dashed contour) by integrating the posteriors. The 1D distributions of M_f and χ_f [Eqs. (7) and (8)] are plotted as red curves in the side panels. For comparison, we repeat the usual full-RD MCMC analysis in Ref. [33] using their `ringdown` package [53]. The white dashed contour shows the 90% credible region of the joint posteriors from the full-RD analysis. The joint distribution is also projected to the subspace of M_f and χ_f , shown as gray shades in the side panels. The white plus sign marks the remnant mass and spin inferred from the full IMR analysis ($M_f^{\text{IMR}} = 68.5M_\odot$, $\chi_f^{\text{IMR}} = 0.69$) [32]. Studies at various Δt_0 times are discussed in our companion paper [50]. All the results are consistent with the conventional full-RD MCMC analysis [33].

Model evidence and Bayes factor.— We compute the model evidence by integrating the likelihoods in Eq. (5)

$$P(d_t|\mathcal{F}_{\text{tot}}, \Delta t_0) = \iint P(d_t|M_f, \chi_f, \Delta t_0, \mathcal{F}_{\text{tot}}) \times \Pi(M_f, \chi_f) dM_f d\chi_f. \quad (9)$$

Assuming a flat prior, the top panel of Fig. 2 shows the evidence as a function of Δt_0 , using $\mathcal{F}_{\text{tot}} = \mathcal{F}_{220}$ (blue) and $\mathcal{F}_{\text{tot}} = \mathcal{F}_{221}\mathcal{F}_{220}$ (red). We see both curves surge quickly around $\Delta t_0 \sim 0$, implying the onset of the ringdown regime, and then level off, followed by oscillations around a plateau. Both curves start to rise before $\Delta t_0 = 0$ because the width of the analysis window 0.2 s is much wider than the ringdown signal; the full ringdown is already in the window even when Δt_0 is still slightly negative. The evidence increases sharply as the inspiral signal slides off the ringdown window. Such a generic trend of the evidence curve around a ringdown signal naturally offers us an agnostic estimate of the start time of a QNM.

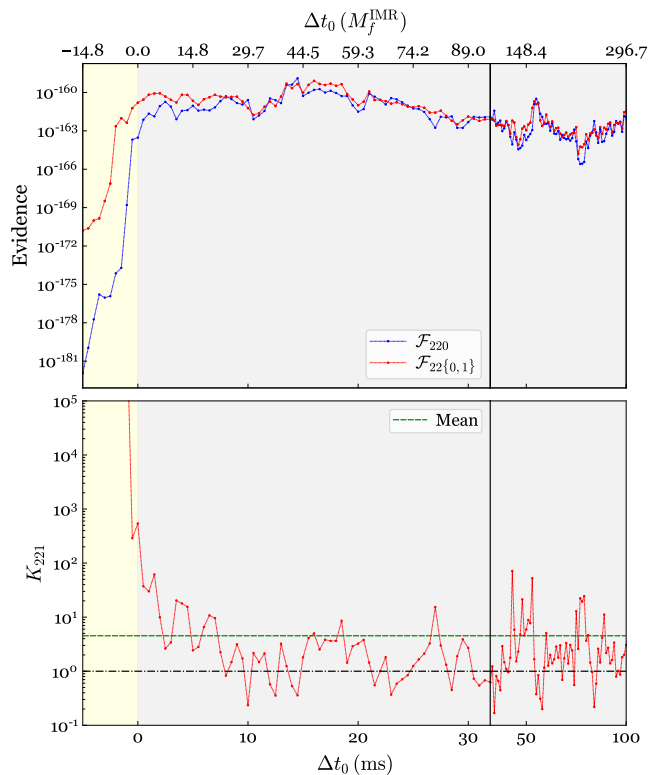


FIG. 2. Model evidence (top) and Bayes factor (bottom) as a function of analysis starting time Δt_0 . In the top panel, the red (blue) curve indicates the results with (without) the first overtone included in the filter. In the bottom panel, the ratio between the two is shown as the Bayes factor [Eq. (10)]. The green dashed line indicates the mean value for $\Delta t_0 \in [15, 100]$ ms. The black dash-dotted line marks the unity.

In addition, we calculate the Bayes factor by taking the ratio of the two evidence curves:

$$K_{221}(\Delta t_0) = \frac{P(d_t|\mathcal{F}_{22\{0,1\}}, \Delta t_0)}{P(d_t|\mathcal{F}_{220}, \Delta t_0)}. \quad (10)$$

The results are plotted in the bottom panel of Fig. 2. We see the value of K_{221} decreases sharply at $\Delta t_0 \lesssim 2$ ms. At later times, it fluctuates around a mean value of 4.5 for $\Delta t_0 \in [15, 100]$ ms, when we expect no ringdown signal remains. We find a Bayes factor as high as 600 at the peak time $\Delta t_0 = 0$, demonstrating strong preference of the existence of the first overtone.

MCMC analysis after mode cleaning.— Detecting a subdominant QNM with the conventional MCMC approach (without mode cleaning) is complicated by the presence of the dominant mode(s), especially at low-SNR regime. We can take advantage of mode cleaning to surmount such challenge. We first apply the rational filter to remove the dominant mode(s), and then use the established criteria (in terms of the standard MCMC) to look for the evidence of the subdominant QNM(s) in the filtered data. This forms a hybrid approach to do BH spectroscopy.

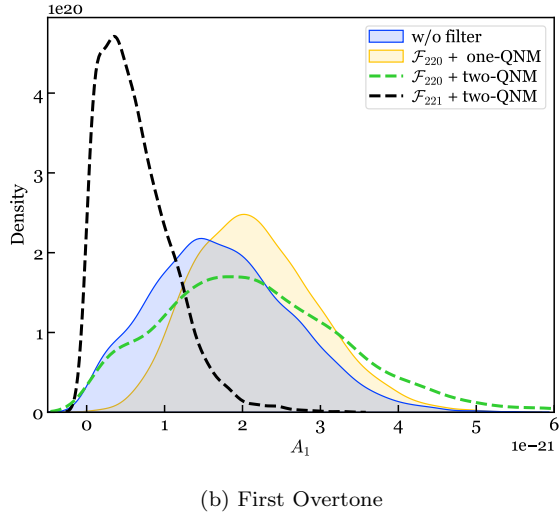
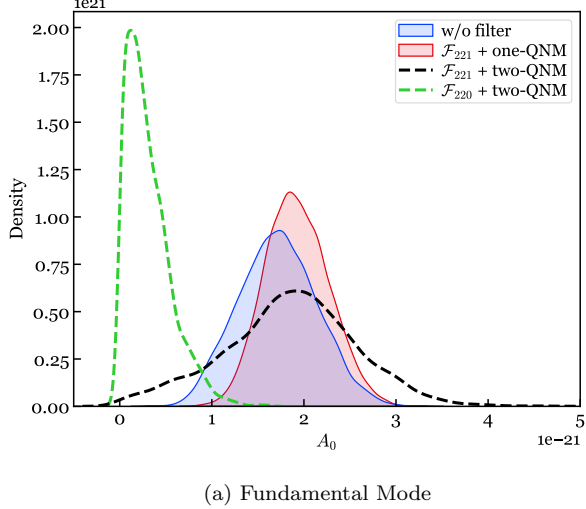


FIG. 3. Posterior distributions of the mode amplitude for the fundamental mode (top) and the first overtone (bottom) in GW150914 ($\Delta t_0 = 0.77$ ms). The blue shaded regions are obtained from the full-RD MCMC analysis (without filters). After cleaning the fundamental mode (applying \mathcal{F}_{220}), the filtered data are fitted with a two-QNM template (green) and an overtone-only template (yellow). Similarly, after cleaning the first overtone (applying \mathcal{F}_{221}), the data are fitted with a two-QNM template (black) and a fundamental-mode-only template (red).

We continue to demonstrate the hybrid approach using GW150914 ($\Delta t_0 = 0.77$ ms). We first analyze the unfiltered data with the conventional full-RD MCMC, using the `ringdown` package [33, 53]. The resulting posteriors of the mode amplitudes are shown as the blue shaded distributions in Fig. 3. Next, we remove the fundamental mode by applying the filter \mathcal{F}_{220} , with M_f and χ_f fixed to the IMR-estimated values. After cleaning the

fundamental mode, we fit the filtered data using MCMC with a two-QNM ringdown template including both the fundamental mode and the first overtone, i.e., assuming we are agnostic of mode cleaning. The results are shown as green dashed curves in Fig. 3. The posterior distribution of the fundamental mode amplitude is pushed to ~ 0 . The distribution of the first overtone amplitude remains unchanged (consistent with the blue distribution). Note that since the filter reduces the amplitude of the first overtone by $B_{220}^{221} = 0.487$ [Eq. (4)], we compensate for this factor in the figure for a fair comparison. The results demonstrate that the fundamental mode is indeed removed. We can also fit the same filtered data with a one-QNM, overtone-only template, which leads to the yellow shaded distribution in Fig. 3b, consistent with both the two-QNM fitting results (green) and the unfiltered data fitting results (blue).

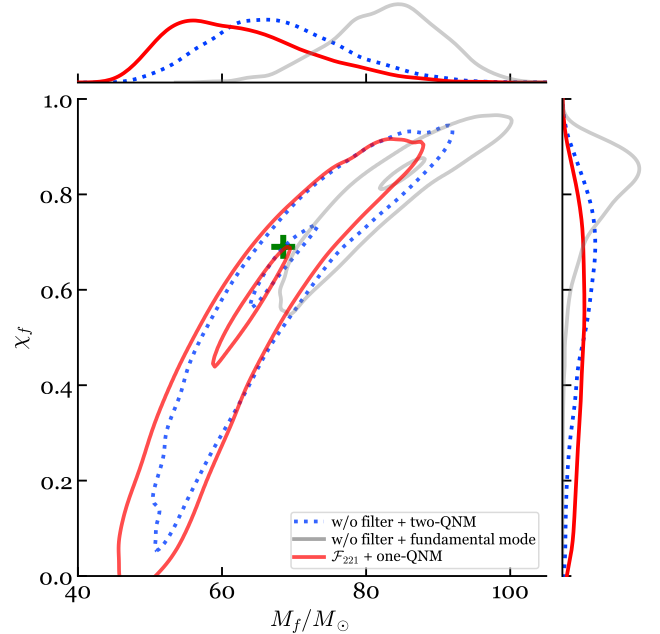


FIG. 4. Posteriors of M_f and χ_f inferred from the ringdown of GW150914 ($\Delta t_0 = 0.77$ ms). The full-RD MCMC approach (without filters) yields the blue dashed contours using a two-QNM model (ω_{220} and ω_{221}) and the gray contours using a fundamental-mode-only template. After cleaning the first overtone, fitting the filtered data using a fundamental-mode-only template leads to the red contours. The green plus sign marks the IMR-estimated values.

Similarly, we repeat the procedure to remove the first overtone using \mathcal{F}_{221} . The black dashed curves and the red shaded region correspond to fitting the filtered data with a two-QNM and a fundamental-mode-only template, respectively. This time, the distribution of the first overtone is pushed to ~ 0 , indicating the removal of the first overtone, whereas the fundamental mode is generally not impacted.

In addition to mode amplitudes, we show the estimates of M_f and χ_f for GW150914 at $\Delta t_0 = 0.77$ ms using the hybrid approach (Figure 4). Here we clean the first overtone by applying \mathcal{F}_{221} and then fit the filtered data with the fundamental-mode-only template. The resulting constraints are shown in red, consistent with the IMR-estimated values (green plus sign), as well as the results obtained from the full-RD MCMC analysis with a two-QNM template (blue). On the contrary, the results are biased when we fit the unfiltered data with the fundamental mode alone (gray), i.e., with solely the fundamental mode, the model is not good enough to describe the ringdown at $\Delta t_0 = 0.77$ ms.

Finally, we present the posteriors of M_f inferred from the first overtone alone at different Δt_0 times (Fig. 5). We set uniform prior in the range of $35M_\odot \leq M \leq 140M_\odot$. At the signal peak ($\Delta t_0 = 0$), the maximum a posteriori (MAP) value of M_f is higher than the estimate obtained from the whole IMR signal (the vertical dashed line), which may indicate the existence of residual signals in addition to the two QNMs (ω_{220} and ω_{221}); see more details in our companion paper [50]. Then the MAP value shifts toward smaller M_f and becomes more consistent with the IMR value at later times. In the end, the distribution flattens and becomes less informative at $\Delta t_0 \gtrsim 1$ ms when most of the overtone signal disappears.

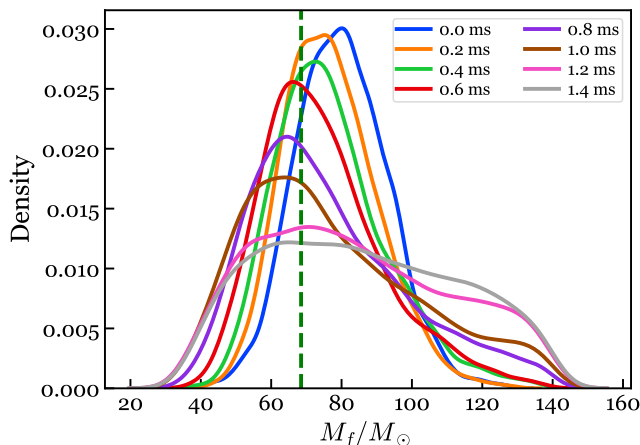


FIG. 5. Posteriors of M_f inferred from the first overtone alone at different starting times. We clean the fundamental mode using the filter \mathcal{F}_{220} and fit the filtered data with the first-overtone-only template. The vertical dashed line indicates the IMR-estimated mass. The colors of the curves correspond to different Δt_0 times (as indicated in the legend).

Discussions.— In this paper, leveraging on rational filters [47], we formulate a mode-cleaning-based Bayesian framework for BH spectroscopy. More details are provided in the companion paper [50]. Complementary to the existing time-domain [33, 45] and frequency-domain studies [55], our new framework has a few advantages.

(a) The rational filters offer a simple way to remove par-

ticular QNM(s) from the ringdown data. After cleaning the most dominant mode(s), the inferences for a subdominant mode become more definitive, especially when the subdominant mode has low SNR.

(b) The filter implicitly marginalizes the likelihoods over mode amplitudes and phases and only depends on the remnant BH’s mass and spin, preventing overfitting when more modes are considered in the ringdown model (Similarly, the filter also avoids overfitting while studying numerical-relativity waveforms [47]). The feature also allows a fully parallelizable pipeline to efficiently evaluate the likelihoods for a wide range of starting times without MCMC, free of technical issues like convergence.

(c) Model evidence is presented as a function of analysis start time. Although the signal peak and the inferred start of ringdown can be obtained from the full IMR analysis, the estimate might degrade when the system configurations and parameters go beyond the available regime of the corresponding IMR waveform model, or when the inspiral signal is too short. The information obtained from the evidence rising time could contribute to the prior distribution of the start time [56] in other frameworks, e.g., Refs. [45, 55].

This work is the first demonstration of an overtone mode in GW150914 after cleaning the fundamental mode. Future application of our framework to other events, e.g., GW190521 [37, 38], and new events in the forthcoming fourth observing run, may lead to discovery and evidence of other modes in BH ringdown. As demonstrated with numerical-relativity waveforms [47], the rational filters provide a powerful tool to reveal subdominant effects, e.g., second-order nonlinearity and retrograde modes. Future detectors will enable us to do BH spectroscopy in a high-SNR regime. Our framework will allow us to test General Relativity and explore the nature of gravity in full detail using real events.

Acknowledgments.— We thank Maximiliano Isi and Will M. Farr for their helpful suggestions and comments. We also thank Eric Thrane, Paul Lasky, Emanuele Berti, Mark Ho-Yeuk Cheung, Roberto Cotesta, and all the attendees of the ringdown workshop held at CCA, Flatiron Institute for useful discussions. Computations for this work were performed with the Wheeler cluster at Caltech. YC and SM acknowledge support from the Brinson Foundation, the Simons Foundation (Award Number 568762), and by NSF Grants PHY-2011961, PHY-2011968, PHY-1836809. LS acknowledges the support of the Australian Research Council Centre of Excellence for Gravitational Wave Discovery (OzGrav), Project No. CE170100004. This material is based upon work supported by NSF’s LIGO Laboratory which is a major facility fully funded by the National Science Foundation.

REFERENCES

- * sma@caltech.edu
- [1] Kostas D. Kokkotas and Bernd G. Schmidt, “Quasinormal modes of stars and black holes,” *Living Rev. Rel.* **2**, 2 (1999), [arXiv:gr-qc/9909058](#).
 - [2] Hans-Peter Nollert, “Quasinormal modes: the characteristic ‘sound’ of black holes and neutron stars,” *Classical and Quantum Gravity* **16**, R159–R216 (1999).
 - [3] Vitor Cardoso and Leonardo Gualtieri, “Testing the black hole ‘no-hair’ hypothesis,” *Class. Quant. Grav.* **33**, 174001 (2016), [arXiv:1607.03133 \[gr-qc\]](#).
 - [4] Emanuele Berti, Vitor Cardoso, and Andrei O. Starinets, “Quasinormal modes of black holes and black branes,” *Class. Quant. Grav.* **26**, 163001 (2009), [arXiv:0905.2975 \[gr-qc\]](#).
 - [5] Roger Penrose, ““golden oldie”: Gravitational collapse: the role of general relativity,” *General Relativity and Gravitation* **34**, 1141–1165 (2002).
 - [6] Piotr T. Chrusciel, Joao Lopes Costa, and Markus Heusler, “Stationary Black Holes: Uniqueness and Beyond,” *Living Rev. Rel.* **15**, 7 (2012), [arXiv:1205.6112 \[gr-qc\]](#).
 - [7] B. Carter, “Axisymmetric black hole has only two degrees of freedom,” *Phys. Rev. Lett.* **26**, 331–333 (1971).
 - [8] Werner Israel, “Event horizons in static vacuum space-times,” *Phys. Rev.* **164**, 1776–1779 (1967).
 - [9] Fernando Echeverria, “Gravitational-wave measurements of the mass and angular momentum of a black hole,” *Phys. Rev. D* **40**, 3194–3203 (1989).
 - [10] Olaf Dreyer, Bernard J. Kelly, Badri Krishnan, Lee Samuel Finn, David Garrison, and Ramon Lopez-Aleman, “Black hole spectroscopy: Testing general relativity through gravitational wave observations,” *Class. Quant. Grav.* **21**, 787–804 (2004), [arXiv:gr-qc/0309007 \[gr-qc\]](#).
 - [11] Emanuele Berti, Vitor Cardoso, and Clifford M. Will, “On gravitational-wave spectroscopy of massive black holes with the space interferometer LISA,” *Phys. Rev. D* **73**, 064030 (2006), [arXiv:gr-qc/0512160 \[gr-qc\]](#).
 - [12] Emanuele Berti, Jaime Cardoso, Vitor Cardoso, and Marco Cavaglia, “Matched-filtering and parameter estimation of ringdown waveforms,” *Phys. Rev. D* **76**, 104044 (2007), [arXiv:0707.1202 \[gr-qc\]](#).
 - [13] S. Gossan, J. Veitch, and B. S. Sathyaprakash, “Bayesian model selection for testing the no-hair theorem with black hole ringdowns,” *Phys. Rev. D* **85**, 124056 (2012), [arXiv:1111.5819 \[gr-qc\]](#).
 - [14] Sarah Caudill, Scott E. Field, Chad R. Galley, Frank Herrmann, and Manuel Tiglio, “Reduced Basis representations of multi-mode black hole ringdown gravitational waves,” *Class. Quant. Grav.* **29**, 095016 (2012), [arXiv:1109.5642 \[gr-qc\]](#).
 - [15] J. Meidam, M. Agathos, C. Van Den Broeck, J. Veitch, and B. S. Sathyaprakash, “Testing the no-hair theorem with black hole ringdowns using TIGER,” *Phys. Rev. D* **90**, 064009 (2014), [arXiv:1406.3201 \[gr-qc\]](#).
 - [16] Swetha Bhagwat, Duncan A. Brown, and Stefan W. Ballmer, “Spectroscopic analysis of stellar mass black-hole mergers in our local universe with ground-based gravitational wave detectors,” *Phys. Rev. D* **94**, 084024 (2016), [Erratum: *Phys. Rev. D* **95**, 069906 (2017)], [arXiv:1607.07845 \[gr-qc\]](#).
 - [17] Emanuele Berti, Alberto Sesana, Enrico Barausse, Vitor Cardoso, and Krzysztof Belczynski, “Spectroscopy of Kerr black holes with Earth- and space-based interferometers,” *Phys. Rev. Lett.* **117**, 101102 (2016), [arXiv:1605.09286 \[gr-qc\]](#).
 - [18] Vishal Baibhav, Emanuele Berti, Vitor Cardoso, and Gaurav Khanna, “Black Hole Spectroscopy: Systematic Errors and Ringdown Energy Estimates,” *Phys. Rev. D* **97**, 044048 (2018), [arXiv:1710.02156 \[gr-qc\]](#).
 - [19] Andrea Maselli, Kostas Kokkotas, and Pablo Laguna, “Observing binary black hole ringdowns by advanced gravitational wave detectors,” *Phys. Rev. D* **95**, 104026 (2017), [arXiv:1702.01110 \[gr-qc\]](#).
 - [20] Huan Yang, Kent Yagi, Jonathan Blackman, Luis Lehner, Vasileios Paschalidis, Frans Pretorius, and Nicolás Yunes, “Black hole spectroscopy with coherent mode stacking,” *Phys. Rev. Lett.* **118**, 161101 (2017), [arXiv:1701.05808 \[gr-qc\]](#).
 - [21] C. F. Da Silva Costa, S. Tiwari, S. Klimentenko, and F. Salemi, “Detection of (2,2) quasinormal mode from a population of black holes with a constructive summation method,” *Phys. Rev. D* **98**, 024052 (2018), [arXiv:1711.00551 \[gr-qc\]](#).
 - [22] Vishal Baibhav and Emanuele Berti, “Multimode black hole spectroscopy,” *Phys. Rev. D* **99**, 024005 (2019), [arXiv:1809.03500 \[gr-qc\]](#).
 - [23] Gregorio Carullo *et al.*, “Empirical tests of the black hole no-hair conjecture using gravitational-wave observations,” *Phys. Rev. D* **98**, 104020 (2018), [arXiv:1805.04760 \[gr-qc\]](#).
 - [24] Richard Brito, Alessandra Buonanno, and Vivien Raymond, “Black-hole Spectroscopy by Making Full Use of Gravitational-Wave Modeling,” *Phys. Rev. D* **98**, 084038 (2018), [arXiv:1805.00293 \[gr-qc\]](#).
 - [25] Hiroyuki Nakano, Tatsuya Narikawa, Ken-ichi Oohara, Kazuki Sakai, Hisa-aki Shinkai, Hirotaka Takahashi, Takahiro Tanaka, Nami Uchikata, Shun Yamamoto, and Takahiro S. Yamamoto, “Comparison of various methods to extract ringdown frequency from gravitational wave data,” *Phys. Rev. D* **99**, 124032 (2019), [arXiv:1811.06443 \[gr-qc\]](#).
 - [26] Miriam Cabero, Julian Westerweck, Collin D. Capano, Sumit Kumar, Alex B. Nielsen, and Badri Krishnan, “Black hole spectroscopy in the next decade,” *Phys. Rev. D* **101**, 064044 (2020), [arXiv:1911.01361 \[gr-qc\]](#).
 - [27] Swetha Bhagwat, Miriam Cabero, Collin D. Capano, Badri Krishnan, and Duncan A. Brown, “Detectability of the subdominant mode in a binary black hole ringdown,” *Phys. Rev. D* **102**, 024023 (2020), [arXiv:1910.13203 \[gr-qc\]](#).
 - [28] Iara Ota and Cecilia Chirenti, “Overtones or higher harmonics? Prospects for testing the no-hair theorem with gravitational wave detections,” *Phys. Rev. D* **101**, 104005 (2020), [arXiv:1911.00440 \[gr-qc\]](#).
 - [29] Juan Calderón Bustillo, Paul D. Lasky, and Eric Thrane, “Black-hole spectroscopy, the no-hair theorem, and GW150914: Kerr versus Occam,” *Phys. Rev. D* **103**, 024041 (2021), [arXiv:2010.01857 \[gr-qc\]](#).
 - [30] Xisco Jiménez Forteza, Swetha Bhagwat, Paolo Pani, and Valeria Ferrari, “Spectroscopy of binary black hole ringdown using overtones and angular modes,” *Phys. Rev. D* **102**, 044053 (2020), [arXiv:2005.03260 \[gr-qc\]](#).
 - [31] B. P. Abbott *et al.* (LIGO Scientific, Virgo), “Tests of general relativity with GW150914,” *Phys. Rev. Lett.* **116**, 221101 (2016), [Erratum: *Phys. Rev.*

- Lett.121,no.12,129902(2018)], [arXiv:1602.03841 \[gr-qc\]](#).
- [32] Maximiliano Isi, Matthew Giesler, Will M. Farr, Mark A. Scheel, and Saul A. Teukolsky, “Testing the no-hair theorem with GW150914,” *Phys. Rev. Lett.* **123**, 111102 (2019), [arXiv:1905.00869 \[gr-qc\]](#).
 - [33] Maximiliano Isi and Will M. Farr, “Analyzing black-hole ringdowns,” (2021), [arXiv:2107.05609 \[gr-qc\]](#).
 - [34] Roberto Cotesta, Gregorio Carullo, Emanuele Berti, and Vitor Cardoso, “On the detection of ringdown overtones in GW150914,” (2022), [arXiv:2201.00822 \[gr-qc\]](#).
 - [35] Maximiliano Isi and Will M. Farr, “Revisiting the ringdown of GW150914,” (2022), [arXiv:2202.02941 \[gr-qc\]](#).
 - [36] Eliot Finch and Christopher J. Moore, “Searching for a ringdown overtone in GW150914,” *Phys. Rev. D* **106**, 043005 (2022), [arXiv:2205.07809 \[gr-qc\]](#).
 - [37] Collin D. Capano, Miriam Cabero, Julian Westerweck, Jahed Abedi, Shilpa Kastha, Alexander H. Nitz, Alex B. Nielsen, and Badri Krishnan, “Observation of a multimode quasi-normal spectrum from a perturbed black hole,” (2021), [arXiv:2105.05238 \[gr-qc\]](#).
 - [38] Collin D. Capano, Jahed Abedi, Shilpa Kastha, Alexander H. Nitz, Julian Westerweck, Miriam Cabero, Alex B. Nielsen, and Badri Krishnan, “Statistical validation of the detection of a sub-dominant quasi-normal mode in GW190521,” (2022), [arXiv:2209.00640 \[gr-qc\]](#).
 - [39] B. P. Abbott *et al.* (LIGO Scientific, Virgo), “Observation of Gravitational Waves from a Binary Black Hole Merger,” *Phys. Rev. Lett.* **116**, 061102 (2016), [arXiv:1602.03837 \[gr-qc\]](#).
 - [40] J. Aasi *et al.* (LIGO Scientific), “Advanced LIGO,” *Class. Quant. Grav.* **32**, 074001 (2015), [arXiv:1411.4547 \[gr-qc\]](#).
 - [41] Benjamin P. Abbott *et al.*, “Sensitivity of the Advanced LIGO detectors at the beginning of gravitational wave astronomy,” *Phys. Rev. D* **93**, 112004 (2016), [Addendum: *Phys.Rev.D* 97, 059901 (2018)], [arXiv:1604.00439 \[astro-ph.IM\]](#).
 - [42] B. P. Abbott *et al.* (LIGO Scientific, Virgo), “GW150914: The Advanced LIGO Detectors in the Era of First Discoveries,” *Phys. Rev. Lett.* **116**, 131103 (2016), [arXiv:1602.03838 \[gr-qc\]](#).
 - [43] Gregory M. Harry (LIGO Scientific), “Advanced LIGO: The next generation of gravitational wave detectors,” *Class. Quant. Grav.* **27**, 084006 (2010).
 - [44] R. Abbott *et al.* (LIGO Scientific, Virgo), “Properties and Astrophysical Implications of the 150 M_{\odot} Binary Black Hole Merger GW190521,” *Astrophys. J.* **900**, L13 (2020), [arXiv:2009.01190 \[astro-ph.HE\]](#).
 - [45] Gregorio Carullo, Walter Del Pozzo, and John Veitch, “Observational Black Hole Spectroscopy: A time-domain multimode analysis of GW150914,” *Phys. Rev. D* **99**, 123029 (2019), [Erratum: *Phys. Rev.D*100,no.8,089903(2019)], [arXiv:1902.07527 \[gr-qc\]](#).
 - [46] Matthew Giesler, Maximiliano Isi, Mark Scheel, and Saul Teukolsky, “Black hole ringdown: the importance of overtones,” *Phys. Rev. X* **9**, 041060 (2019), [arXiv:1903.08284 \[gr-qc\]](#).
 - [47] Sizheng Ma, Keefe Mitman, Ling Sun, Nils Deppe, François Hébert, Lawrence E. Kidder, Jordan Moxon, William Throwe, Nils L. Vu, and Yanbei Chen, “Quasinormal-mode filters: A new approach to analyze the gravitational-wave ringdown of binary black-hole mergers,” *Phys. Rev. D* **106**, 084036 (2022), [arXiv:2207.10870 \[gr-qc\]](#).
 - [48] Keefe Mitman *et al.*, “Nonlinearities in black hole ringdowns,” (2022), [arXiv:2208.07380 \[gr-qc\]](#).
 - [49] Mark Ho-Yeuk Cheung *et al.*, “Nonlinear effects in black hole ringdown,” (2022), [arXiv:2208.07374 \[gr-qc\]](#).
 - [50] Sizheng Ma *et al.*, the companion paper, in preparation (2022).
 - [51] B. P. Abbott *et al.* (LIGO Scientific, Virgo), “GWTC-1: A Gravitational-Wave Transient Catalog of Compact Binary Mergers Observed by LIGO and Virgo during the First and Second Observing Runs,” *Phys. Rev. X* **9**, 031040 (2019), [arXiv:1811.12907 \[astro-ph.HE\]](#).
 - [52] LIGO Scientific Collaboration and Virgo Collaboration, “Gravitational Wave Open Science Center,” <https://www.gw-openscience.org>.
 - [53] Maximiliano Isi and Will Meierjürgen Farr, “max-isi/ringdown: Initial ringdown release,” (2021).
 - [54] P. Welch, “The use of fast fourier transform for the estimation of power spectra: A method based on time averaging over short, modified periodograms,” *IEEE Transactions on Audio and Electroacoustics* **15**, 70–73 (1967).
 - [55] Eliot Finch and Christopher J. Moore, “Frequency-domain analysis of black-hole ringdowns,” *Phys. Rev. D* **104**, 123034 (2021), [arXiv:2108.09344 \[gr-qc\]](#).
 - [56] Note that the prior distribution of the start time is not needed in our approach.